Experimental determination of pair interaction energies in a $CoPt_3$ single crystal and phase-diagram calculations

E. Kentzinger,* V. Parasote, V. Pierron-Bohnes, J. F. Lami, and M. C. Cadeville
IPCMS-GEMME, CNRS, Université Louis Pasteur, 23 rue du Loess, 67037 Strasbourg, France

J. M. Sanchez
Texas Materials Institute, University of Texas, Austin, Texas 78712

R. Caudron
LEM (ONERA-CNRS), 29 avenue de la Division Leclerc, BP 72, 92320 Châtillon-sous-Bagneux, France and Léon Brillouin Laboratory (CEA-CNRS), CE-Saclay, 91190 Gif sur Yvette, France

B. Beuneu
Laboratoire des Solides Irradiés, CEA–Ecole Polytechnique, 91128 Palaiseau, France and Léon Brillouin Laboratory (CEA-CNRS), CE-Saclay, 91190 Gif sur Yvette, France

(Received 18 November 1999)

The short-range order in a $CoPt_3$ single crystal at 1083 K was measured using neutron diffuse scattering in the (100) and (110) reciprocal planes. The data were used in conjunction with the inverse cluster variation method in order to extract the first four and the sixth effective pair interaction energies. The interactions obtained from the experimental short-range order intensities are used to calculate the Pt-rich side of the phase diagram using the cluster variation method, the order-disorder transition temperature at the stoichiometric composition by Monte Carlo simulations, and the unrelaxed antiphase boundary energies. The agreement with experimental data is excellent. Comparison of the $CoPt_3$ pair energies with those similarly obtained in Co_3Pt by other authors shows an important dependence of the nearest-neighbor pair interaction with concentration.

I. INTRODUCTION

The calculation of binary alloy phase diagrams requires the implementation of accurate electronic structure calculations in order to obtain pair and multisite atomic interactions combined with statistical mechanics techniques such as Monte Carlo simulations or the cluster variation method (CVM). Recently the CVM was reformulated to take into account the contribution of atomic displacements from lattice points,[1] and much attention has been devoted to the contribution of the vibrational entropies to phase stability.[2–7]

Parallel to the theoretical studies, significant effort has been invested in the experimental determination of the effective interactions, static displacements and vibrational entropies in metallic alloys. For the first two quantities, studies of elastic neutron diffuse scattering have focused on the examination of single crystals in thermodynamic equilibrium for systems where the phase diagram is well known or relatively simple such as Ni-V,[8–10] Pd-V,[8,9,11] Pt-V,[11,12] Ni-Cr,[13–16] Fe-V,[17] Fe-Al,[18–21] Cu-Au,[22,23] and Ni-Al.[24] With regard to vibrational entropies, inelastic neutron scattering and cryogenic calorimetry were used in both single and polycrystals.[25–28]

The system investigated here, Co-Pt, offers some interesting aspects. First, its phase diagram, as the classical Au-Cu diagram, is a prototype one, the $L1_2$- and $L1_0$-ordered phases extending around AB_3 and AB concentrations,[29–34] with a notable asymmetry in the stabilities of the Co_3Pt and $CoPt_3$ phases. Secondly, Co-Pt is strongly ferromagnetic on the Co-rich side. The presence of magnetism has long been considered as responsible for the asymmetry of the order disorder transitions. The Co-Pt phase diagram was previously calculated[35] in the tetrahedron approximation of the CVM, that included pair and many-body interactions and magnetic exchange interactions that are sensitive to the local chemical environment. A good agreement with the experimental phase diagram was obtained, with multiplet interactions found to play an important role in the asymmetry of the phase diagram. This phenomenological model assumes concentration independent chemical interactions. An alternative approach is to include the effect of multiplet interactions as a concentration dependence in the pair interactions. Electronic structure calculations in transition metal alloys reveal that these pair interactions are strongly dependent on the filling of the *d* band.[36] Thus, measurement of diffuse intensity in alloys in thermodynamic equilibrium at several stoichiometries, from which concentration dependent pair interactions can be obtained, is a subject of considerable practical and theoretical interest.

Two groups have undertaken this long and delicate measurement at two compositions: the LURE-CECM group using synchrotron radiation diffuse scattering[37] at the Co_3Pt stoichiometry and our group through neutron diffuse scattering at the $CoPt_3$ stoichiometry. Moreover, inelastic neutron-scattering measurements were also performed on another $CoPt_3$ single crystal to get the phonon dispersion spectra at various temperatures in both ordered and disordered states with the aim to determine the contribution of the vibrational

entropy to phase stability and to calculate the atomic migration enthalpies.[38,39]

In this paper we describe high-temperature neutron-diffuse-scattering measurements. Inelastic-scattering measurements is the subject of a forthcoming publication. First we present a brief summary of the experimental procedure (Sec. II), followed by a description of the results in terms of short-range-order (SRO) parameters (Sec. III). In Sec. IV, the effective pair interactions are calculated using the inverse cluster variation method. The results are then used to calculate the Pt-rich side of the equilibrium phase diagram using the CVM. Monte Carlo simulations are also carried out at the stoichiometric composition (Sec. V). The energy of ideal (unrelaxed) conservative antiphase boundary energies along [100] and [111] planes are calculated in Sec. VI. Concluding remarks are given in Sec. VII.

II. EXPERIMENTAL PROCEDURE

The $CoPt_3$ single crystal, lent to us by Professor Cohen (Evanston, Illinois, USA),[40] consisted of a portion of a sphere, 4.13 ± 0.14 mm in diameter and 5.12 ± 0.07 mm high, oriented approximately along the [551] direction. Its composition, determined by chemical analysis, is 75 ± 1 *at.*% platinum. The uncertainty on the composition is due to a composition gradient along its growth direction.

The diffuse intensity measurements were carried out on the G44 two-axis spectrometer at Léon Brillouin Laboratory (CEA-CNRS, Saclay-France). The detection device is composed of 64 He^3 individual detectors : 48 detectors (50 mm in diameter) placed every 2.5° and 16 smaller ones (10 mm in diameter) placed every 0.625°. By rotating the sample in steps of $\Delta\omega = 4°$, a large region of the scattering plane is scanned. We used an incident wavelength of 0.259 nm. The scanned region is then contained between the circles of radii 0.2 and 2.8 reciprocal lattice units (RLU) ($1\ \mathrm{RLU} = 2\pi/a$). The measurements were carried out on the (100) and (110) planes by tilting the single crystal revolution axis from the vertical by $-23.2°$ and 21.8° respectively. This leads to respectively a sampling mesh of 1400 and 1800 measurements points in these planes.

The measurements were taken at 1083 K using a high-temperature furnace located at the center of a 80 cm diameter vacuum vessel. Placing the crystal under vacuum results in significant reduction of the background intensity. At the temperature investigated, which falls above both the order-disorder and the Curie temperatures of the alloy, thermodynamic equilibrium is reached within one second.[41]

Phonon annihilation processes play an important role in neutron scattering. An energy analysis is necessary in order to reject their contribution to the measured intensity. It was performed using a time of flight system. Due to the large incident wavelength (i.e., the low neutron energy), the dominant process is phonon annihilation and the spectra show inelastic scattering essentially on the high-energy side, except in the close vicinity of the Bragg peaks. To get the elastic contribution, we have used the method reported by Barberis in his Ph.D. thesis.[42] It is based on a deconvolution of the time-of-flight spectra from the impulse response of the spectrometer. The result of the deconvolution is a linear combination of a Dirac peak and gaussians to approximate the elastic and inelastic contributions respectively. The impulse response was obtained by measuring a vanadium probe at room temperature. This method is an improvement with respect to the one used before at IPCMS-GEMME (Ref. 17) as it allows the separation of the elastic contribution at wave vectors closer to the Bragg peaks, where the inelastic scattering results essentially from the interaction with low-energy acoustical phonons.[21]

The scattering cross sections were deduced from the weight of the elastic contribution with standard corrections for instrumental background (empty furnace). In order to calibrate the detector response, the scattering cross section by a vanadium sample having the same shape, dimensions, and position in the furnace was measured at room temperature. Some detectors gave erratic results near the polycrystalline peaks of the furnace and, therefore, the corresponding data points were eliminated.

The multiple scattering corrections have been calculated according to Blech and Averbach formulas,[43] the integration inside the portion of a sphere being obtained by a Monte Carlo method. As cobalt and platinum strongly absorb the neutron flux, and cobalt and vanadium have large incoherent cross sections, these correction factors are very strong and anisotropic. They had thus to be evaluated accurately. The absorption corrections for $CoPt_3$ and vanadium have been calculated by a Monte Carlo method considering all possible paths of a neutron inside the volume [$\sigma_{\mathrm{abs}}^{\mathrm{Co}} = 53.56(6)$ b, $\sigma_{\mathrm{abs}}^{\mathrm{Pt}} = 14.84(3)$ b, $\sigma_{\mathrm{abs}}^{\mathrm{V}} = 7.32(6)$ b]. For our $CoPt_3$ sample, the transmission coefficient ranges between 0.20(1) and 0.37(4).

The Debye-Waller attenuation corrections have been evaluated for $CoPt_3$ and vanadium at their respective measurement temperatures. The vanadium Debye-Waller coefficient at room temperature ($B_V = 0.0046$ nm^2) is deduced from its Debye temperature[44] using the Krivoglaz method.[45] The $CoPt_3$ Debye-Waller coefficient at 1083 K [$B_{\mathrm{CoPt_3}} = 0.0108(6)$ nm^2] has been deduced from Berg and Cohen x-ray measurements on the same sample at room temperature,[40] using an harmonic approximation. The deviation between the real Debye-Waller factor and this rough estimate has been deduced from the adjustment of the data in a second step (Sec. III).

The incoherent scattering of the sample and of the vanadium was calculated using $\sigma_{\mathrm{inc}}^{\mathrm{Co}} = 4.8(3)$ b, $\sigma_{\mathrm{inc}}^{\mathrm{Pt}} = 0.13(11)$ b, and $\sigma_{\mathrm{inc}}^{\mathrm{V}} = 5.08(6)$ b for the incoherent scattering cross sections of Co, Pt, and V, respectively.[46] Hence, for the alloy, we get $\sigma_{\mathrm{inc}}^{\mathrm{alloy}} = 1.30(16)$ b. The Laue cross section is $4\pi F_{\mathrm{Laue}} = 1.19(9)$ b where F_{Laue} is the usual normalization factor given by $F_{\mathrm{Laue}} = c(1-c)(b_{\mathrm{Co}} - b_{\mathrm{Pt}})^2$, with c the cobalt concentration, and b_{Co} and b_{Pt} the coherent scattering lengths of Co and Pt, respectively. The incoherent scattering is thus expected to be 1.09(24) in Laue units ($1\ \mathrm{LU} = 4\pi F_{\mathrm{Laue}}$).

III. SHORT-RANGE ORDER PARAMETERS

The experimental cross sections in the two planes investigated are displayed on Fig. 1. SRO is still important at 1083 K. The measured intensity is mostly concentrated near [100] and equivalent points, reaching 5.5 LU at these points.

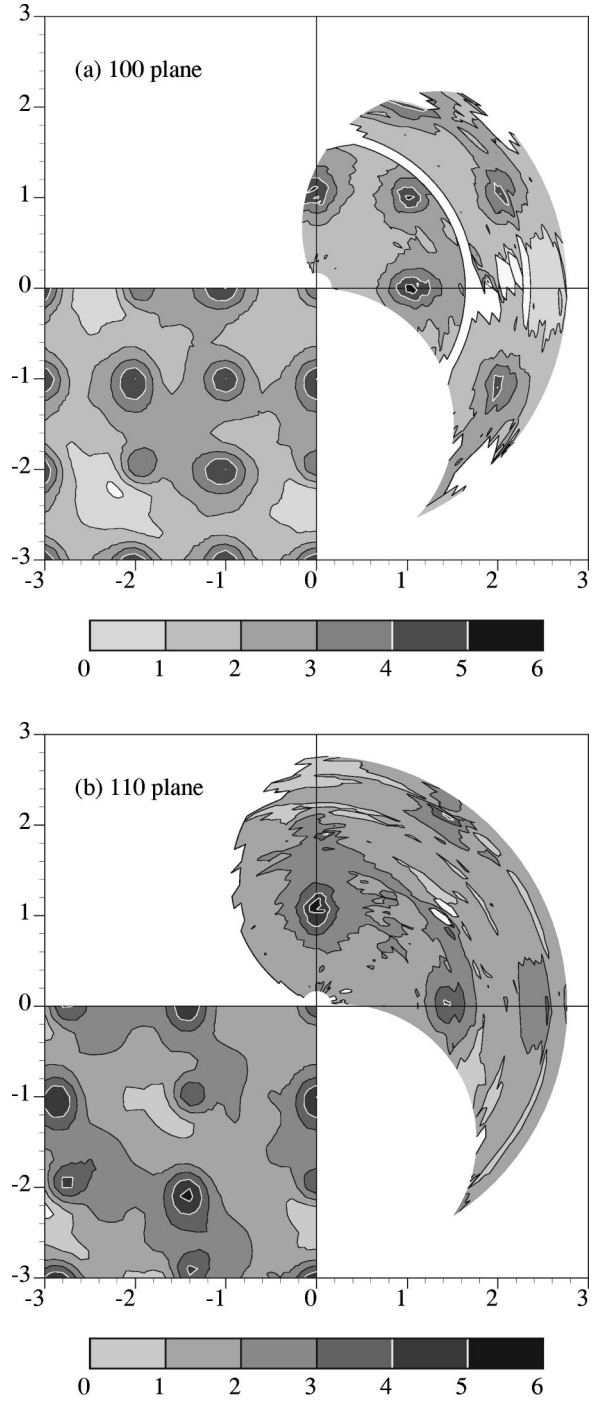

FIG. 1. Corrected experimental intensities at $T=1083$ K and reconstructed ones in the [100] (a) and [110] (b) planes. In each sub- figure, the reconstructed map (down left) has to be compared to the measurement, taking into account the symmetries of the plane.

This very strong modulation means that the transition temperature is not far. The [100] location of the SRO intensity is the signature of a highly stable $L1_2$ phase. The static displacements give rise to a weak asymmetry of the diffuse peaks.

The cross sections were analyzed using the Borie and Sparks[47] formulation. With corrections for temperature attenuation given by the Debye-Waller factor B_{CoPt_3}, the corrected intensity in Laue units is written

$$I_{\mathrm{corr}}(\vec{k})=\frac{1}{NF_{\mathrm{Laue}}}\left[\frac{d\sigma}{d\Omega}(\vec{k})e^{(B_{\mathrm{CoPt_3}}k^2/8\pi^2)}\right], \tag{1}$$

where N is the total number of atoms in the beam.

Up to first order in the atomic displacements $\vec{u}_{\mathbf{p}}$ at lattice site $\vec{R}_{\mathbf{p}}=a/2(p_1,p_2,p_3)$, where $\mathbf{p}$ stands for the set of integers (p_1,p_2,p_3), the corrected intensity at the reciprocal space point $\vec{k}=2\pi/a(h_1,h_2,h_3)$ is given by

$$I_{\mathrm{corr}}(\vec{k})=\alpha(\vec{k})+\sum_{i=1}^{3} h_iQ_i(\vec{k})+I_{\mathrm{inc}}, \tag{2}$$

where $\alpha(\vec{k})$ is the SRO contribution, the $Q_i(\vec{k})$ are related to the Fourier transform of the atomic displacements and I_{inc} is the incoherent scattering per atom in Laue units.

The SRO intensity is given by the Fourier transform of the Warren-Cowley SRO parameters $\alpha_{\mathbf{p}}$:[48]

$$\alpha(\vec{k})=\sum_{\mathbf{p}} \alpha_{\mathbf{p}}\cos(\vec{k}\cdot\vec{R}_{\mathbf{p}}) \tag{3}$$

with the Warren-Cowley SRO parameters defined by

$$\alpha_{\mathbf{p}}=\frac{\langle\sigma_{\mathbf{o}}\sigma_{\mathbf{p}}\rangle-\langle\sigma_{\mathbf{o}}\rangle^2}{1-\langle\sigma_{\mathbf{o}}\rangle^2}, \tag{4}$$

where $\sigma_{\mathbf{o}}$ and $\sigma_{\mathbf{p}}$ are occupation operators at the origin and site $\mathbf{p}$, respectively. These occupation operators take values 1 or -1 if the lattice site is respectively occupied by Co or Pt atoms, and the brackets $\langle\ \rangle$ stand for configurational averages. Equation (3) contains the α_0 term whose theoretical value is 1.

The quantities $\vec{Q}(\vec{k})=[Q_1,Q_2,Q_3]$ in Eq. (2) are given by the first order displacement parameters $\vec{\gamma}_{\mathbf{p}}$:

$$\vec{Q}(\vec{k})=\sum_{\mathbf{p}} \vec{\gamma}_{\mathbf{p}}\sin(\vec{k}\cdot\vec{R}_{\mathbf{p}}). \tag{5}$$

In turn, the displacement parameters $\vec{\gamma}_{\mathbf{p}}$ are defined by

$$\vec{\gamma}_{\mathbf{p}}=-\frac{2\pi}{a}\sum_{\sigma\sigma'}\frac{b_\sigma b_{\sigma'}}{F_{\mathrm{Laue}}}\rho_{2,\mathbf{p}}(\sigma\sigma')\langle\Delta\vec{u}_{\mathbf{p}}^{\sigma\sigma'}\rangle, \tag{6}$$

where $\langle\Delta\vec{u}_{\mathbf{p}}^{\sigma\sigma'}\rangle$ is the average relative displacement between atoms of type σ and σ' (i.e., Co or Pt) separated by $\vec{R}_{\mathbf{p}}$, and where $\rho_{2,\mathbf{p}}(\sigma\sigma')$ is the probability of finding atoms σ and σ' at a distance $\vec{R}_{\mathbf{p}}$. We note that these probabilities are $c^2+c(1-c)\alpha_{\mathbf{p}}$, $(1-c)^2+c(1-c)\alpha_{\mathbf{p}}$, and $c(1-c)-c(1-c)\alpha_{\mathbf{p}}$ for CoCo, PtPt, and CoPt pairs, respectively.

A set of Warren-Cowley SRO parameters and of first-order displacement parameters were fitted to the corrected data using a least squares procedure with a weight inversely proportional to the square of the experimental error ΔI. Thus, the residual error to be minimized is

$$\chi^2=\sum\frac{(I_{\mathrm{measured}}-I_{\mathrm{calculated}})^2}{N_{\mathrm{freedom}}\cdot\Delta I^2}, \tag{7}$$

where $N_{\mathrm{freedom}}=N_{\mathrm{points}}-N_{\mathrm{variables}}$ is the number of degrees of freedom of the fit, N_{points} is the number of experimental points (around 3000).

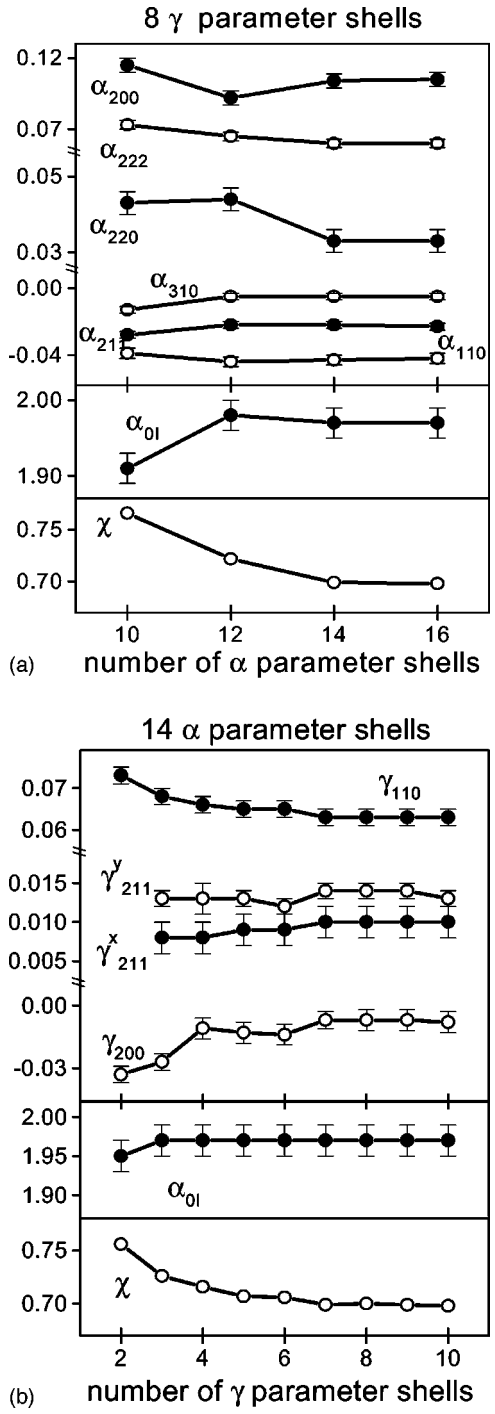

FIG. 2. (a) Sensitivity of the SRO parameters α_n, the constant contribution α_{0I} and the residual error χ to the number of SRO parameters in the fit. (b) Sensitivity of the displacement parameters γ_n, the constant contribution α_{0I} and the residual error χ to the number of displacement parameters in the fit.

We have varied the number of shells for the SRO parameters up to 16, and those for the displacements up to 10. The sensitivity of the results to the number of SRO parameters or to the number of displacement parameter shells is shown on Fig. 2. Above 14 SRO parameters, the residual error does not vary significantly and all the calculated cross sections are qualitatively the same, indicating that the parameters are stable. With regard to the displacement parameters, all results are stable above 7 shells. We discuss now the results

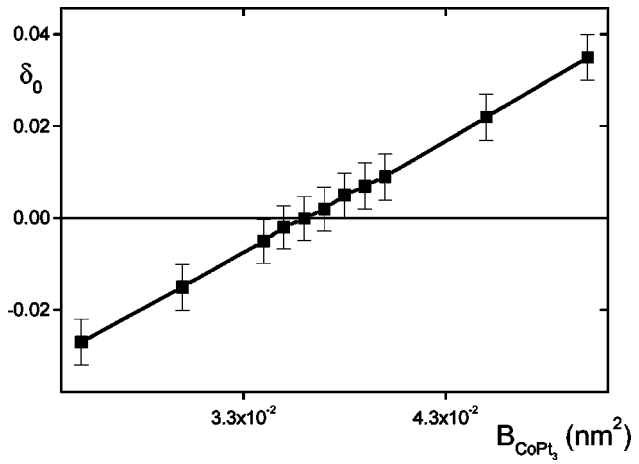

FIG. 3. Sensitivity of the δ_O parameter to the Debye-Waller factor.

analyzed with 14 shells for the SRO parameters and 7 shells for the displacement parameters.

As already mentioned, the Debye-Waller factor used initially is very rough since we have extrapolated the value measured by Berg and Cohen at room temperature in an harmonic approximation to estimate the value of $B_{\mathrm{CoPt_3}}$ at the SRO measurement temperature. Moreover, it is expected that the attenuation of the diffuse scattering and of the Bragg peaks are not equal in the presence of static displacements, since the sign in front of the static Debye-Waller contribution is different in the two cases (decreasing B for SRO).[49] To take into account a possible difference between the applied correction and the real Debye-Waller attenuation (δB), we added in Eq. (2) a term of the form $\delta_0 k^2$ [expansion to first order in δB of the term $e^{(Bk^2/8\pi^2)}$ of Eq. (1)] and fitted δ_0 to the experimental data. The Debye-Waller factor was corrected until the value of δ_0 resulting from the fit was zero (Fig. 3). The corresponding value of $B_{\mathrm{CoPt_3}}$ is very near to the initial estimate [$B_{\mathrm{CoPt_3}}=0.0109(3)$ nm^2 compared to 0.0108(6) nm^2], despite the expected deviation from the harmonic law at this temperature, which is significantly higher than the $CoPt_3$ Debye temperature. Thus, we conclude that the effect of static displacements and the effect of the deviation from the harmonic law compensate each other almost exactly.

The constant contribution to the cross section, α_{0I}, is the sum of the $\alpha_0=1$ term and the sample incoherent contribution. Its expected value is thus 2.09(24) LU. We obtain 1.97(2) LU, which is smaller than the expected value by a factor of 1.06, but remains within the error bar. Other authors[8,9] also observed a discrepancy between the experimental and theoretical values of α_{0I}. They attributed it to errors in the evaluation of the number of atoms in the beam, and proceeded to renormalize all the data. In our case, some differential dilatation of the sample holder and the slit holder could be the source of a partial displacement of the sample out of the beam. Since the sample is small, one half millimeter shift would explain such a discrepancy. As this correction is linear and totally independent from the others, we also renormalized the data and, thus, the values of the α_n (Fig. 4) and γ_n that are given in Tables I and II are corrected by this factor 1.06.

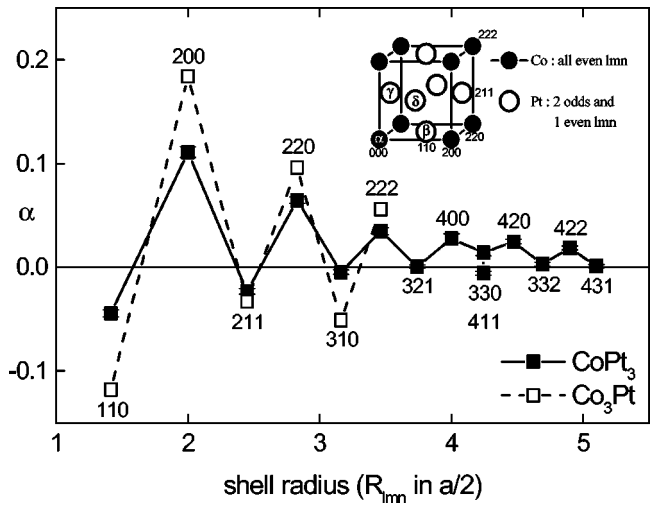

FIG. 4. Variation of the Warren-Cowley SRO parameters with the distance in $CoPt_3$ (present work) and Co_3Pt (Ref. 37). In inset: the $L1_2$ ordered phase with the different atomic occupations on the four sublattices α to δ.

In absolute values, the largest parameters are α_2 and α_4, with a strong attractive order between second and fourth neighbor like atoms. Up to the eighth neighbors, the signs of the SRO parameters are in agreement with the nature of the pairs observed in the $L1_2$ ordered phase (inset, Fig. 4), i.e., heterochemical first, third, fifth and seventh neighbor pairs, and homochemical second, fourth, sixth and eighth neighbor pairs (all even lmn).

The γ_n values are much smaller than those determined in similar systems as VPt_3 Ref. 12 or Ni-V.[10] This is surprising as the relative difference of atomic volume is higher in the Co-Pt system (36%) than in Pt-V (5%) and Ni-V (8%).

The cross sections reconstructed using Eq. (2) are shown on Fig. 1. Taking into account the experimental errors (0.2 LU on average), the results of the adjustment are in good agreement with the experimental data. The diffuse intensity is nearly symmetrical around the [100] points, which is also indicative of small displacement contributions.

TABLE I. Experimental short range order parameters, pair interaction energies, and corresponding error bars on the order-disorder critical temperature calculated in Sec. V B.

i	lmn	α_i	$\Delta\alpha_i$	V_i (meV)	ΔV_i (meV)	$\Delta T_{CO}(K)$
1	110	−0.0444	0.0034	3.76	0.70	24
2	200	0.1110	0.0052	−7.73	1.07	56
3	211	−0.0240	0.0025	1.11	0.43	30
4	220	0.0635	0.0030	−3.17	0.76	79
5	310	−0.0050	0.0023			
6	222	0.0345	0.0033	−0.29	0.80	56
7	321	0.0011	0.0016			
8	400	0.0293	0.0046			
9	330	0.0136	0.0028			
10	411	−0.0057	0.0020			
11	420	0.0241	0.0022			
12	332	0.0027	0.0020			
13	422	0.0191	0.0020			
14	431	0.0007	0.0014			

TABLE II. Displacement parameters (for $i>7$ the values are within the error bar).

i	γ_{ix}	$\Delta\gamma_{ix}$	γ_{iy}	$\Delta\gamma_{iy}$	γ_{iz}	$\Delta\gamma_{iz}$
1	0.0615	0.0023	0.0615	0.0023		
2	−0.0088	0.0056				
3	0.0108	0.0019	0.0135	0.0015	0.0135	0.0015
4	−0.0111	0.0026	−0.0111	0.0026		
5	0.0063	0.0023	0.0039	0.0021		
6	−0.0037	0.0021	−0.0037	0.0021	−0.0037	0.0021
7	0.0068	0.0014	−0.0003	0.0014	−0.0007	0.0014

IV. EFFECTIVE PAIR INTERACTIONS

In order to extract the effective pair interactions from the experimental values of the Warren-Cowley SRO parameters, we consider a simple Ising Hamiltonian for the alloy in which the magnetic moments are localized on the Co atoms:

$$H_0=\frac{1}{2}\sum_{\mathbf{p},\mathbf{p}'} V^c_{\mathbf{pp}'}\sigma_{\mathbf{p}}\sigma_{\mathbf{p}'}-\frac{1}{8}\sum_{\mathbf{p},\mathbf{p}'} J_{\mathbf{pp}'}(1+\sigma_{\mathbf{p}})(1+\sigma_{\mathbf{p}'})S_{\mathbf{p}}S_{\mathbf{p}'}, \tag{8}$$

where $S_{\mathbf{p}}=\pm 1$ is the spin at site $\vec{R}_{\mathbf{p}}$. In Eq. (8), $V^c_{\mathbf{pp}'}$ and $J_{\mathbf{pp}'}$ are, respectively, effective chemical and exchange interactions between sites $\vec{R}_{\mathbf{p}}$ and $\vec{R}_{\mathbf{p}'}$. Averaging over the magnetic degrees of freedom, the interacting part of the alloy Hamiltonian can be written as

$$H_2=\frac{1}{2}\sum_{\mathbf{p},\mathbf{p}'} \tilde{V}_{\mathbf{pp}'}\sigma_{\mathbf{p}}\sigma_{\mathbf{p}'}, \tag{9}$$

where the effective pair interaction is

$$\tilde{V}_{\mathbf{pp}'}=V^c_{\mathbf{pp}'}-\frac{1}{4}J_{\mathbf{pp}'}\langle S_{\mathbf{p}}S_{\mathbf{p}'}\rangle. \tag{10}$$

As observed in our previous study of the Fe-Al system, where the interplay between chemical and magnetic SRO is also present,[20] the effective pair interactions vary appreciably with temperature near the Curie temperature. However, in the limit of high temperatures, the $\tilde{V}_n$ tend to V^c_n as the magnetic SRO parameters $\langle S_{\mathbf{p}}S_{\mathbf{p}'}\rangle$ become negligible. The temperature investigated here (1083 K) is very high compared to the Curie temperature ($T_c=288$ K) (Refs. 29,30) of the $CoPt_3$ alloy. Thus, the effect of magnetic SRO on the pair interactions should be small. Note that in terms of the interaction energies between different chemical species, the effective interactions are given by

$$\tilde{V}_{\mathbf{pp}'}=\frac{1}{4}[\tilde{V}^{\mathrm{CoCo}}_{\mathbf{pp}'}+\tilde{V}^{\mathrm{PtPt}}_{\mathbf{pp}'}-2\tilde{V}^{\mathrm{CoPt}}_{\mathbf{pp}'}]. \tag{11}$$

In order to extract the effective interactions from the experimental diffuse scattering, we fitted the Warren-Cowley SRO parameters using the inverse cluster variation method (CVM) algorithm proposed by Gratias and Cénédèse.[50] The CVM approximation used in the inverse method includes two maximum clusters: the face-centered cube and the 13-point cubo-octahedron.[51] In this approximation, which we

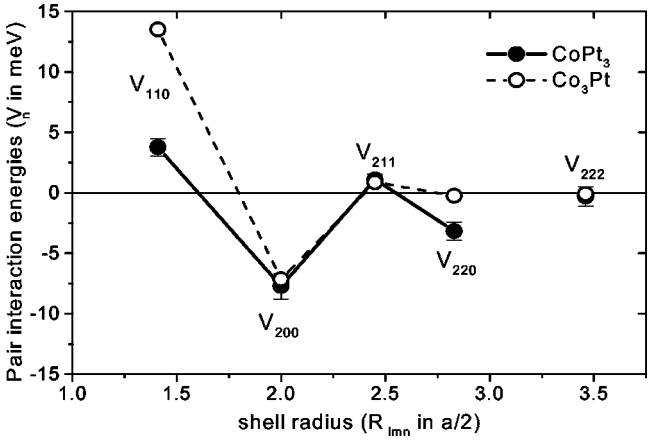

FIG. 5. Pair interaction energies in $CoPt_3$ compared to those in the Co_3Pt alloy (Ref. 37).

will refer to as the 13-14 approximation, we are able to compute the first four and the sixth effective interactions in the fcc lattice. The results of the inverse CVM applied to $CoPt_3$ are presented in Table I and Fig. 5.

One point to be noticed is that, whereas the transition temperature is quite high in this compound (978 K), the value of the first neighbor pair interaction energy V_1 is very small. This can be explained by the fact that the signs of the pair interactions are such that they favor the correct site occupation of the $L1_2$ ordered phase (inset of Fig. 4): negative V_{lmn} for all even lmn, positive V_{lmn} otherwise. Thus, the interactions at all distances reinforce the order and there is no competition between the different pairs.

On Fig. 5 are also plotted the results obtained by the LURE group in the Co_3Pt system.[37] We can see that the main difference is a factor of 3 between the first neighbor pair interaction values. The signs and amplitudes of the other pair interactions are very similar otherwise. As the Co_3Pt system has been measured in the ferromagnetic state (the Curie temperature in this system is higher than the order-disorder critical temperature), the magnetic contribution to the effective pair interaction diminishes the first pair interaction energy so that the chemical part of interactions in Co_3Pt should be even higher than the value measured by the LURE group in the ferromagnetic state. Thus an important dependence of the first neighbor pair interactions with concentration is observed in the Co-Pt system.

The concentration dependence of pair interactions and the fact that V_1 is smaller than V_2 can be explained by the electronic structure calculations of multiatom interactions in transition metal alloys of Bieber and Gautier.[36] These calculations predict an oscillating behavior of the interactions with the d-band filling and, therefore, one might expect that V_1 and V_2 may be of the same magnitude near the nodes of V_1. Likewise, the calculations predict a strong concentration dependence of the interactions.

V. CALCULATIONS OF THE ORDER-DISORDER TRANSITION TEMPERATURES

A. CVM calculation of the phase diagram

The Pt-rich side of the phase diagram was calculated using the CVM approximation described in Sec. IV, in which

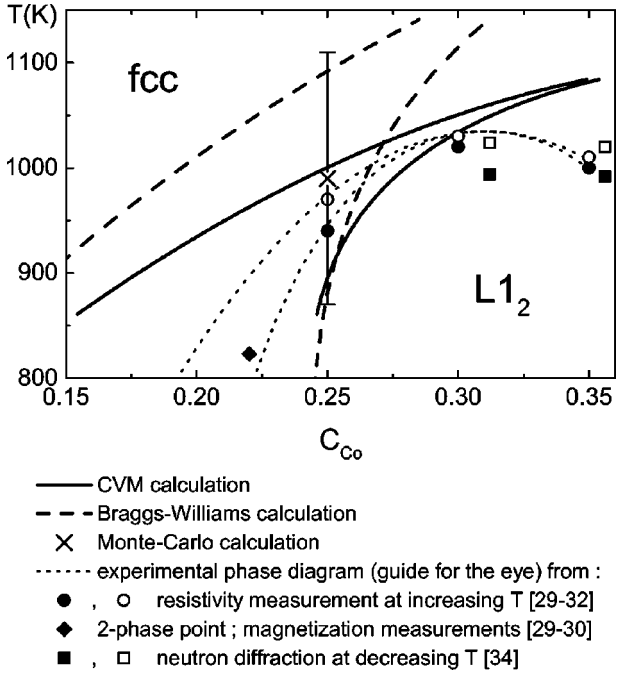

FIG. 6. Comparison of calculated and experimental phase diagrams on the Pt-rich side.

the two maximum clusters are the face-centered cube and the 13-point cubo-octahedron. The same portion of the phase diagram was also calculated in the Bragg-Williams approximation. The results are given in Fig. 6 for the concentration range between 15 and 35 % cobalt.

The figure also contains all the available experimental data in this concentration range obtained using magnetization and resistivity measurements for increasing temperature[29–32] and neutron-diffraction measurement for decreasing temperature.[34] The discrepancy between both sets of data can be explained by the hysteresis of the order-disorder transition and by kinetics effects.

The agreement between the experimental data and the calculated transition temperatures in both approximations is very good. In this regard, we note that the uncertainty in the calculated transition temperatures due to errors in the pair interactions is at least 100 K (it can be estimated using the Clapp and Moss formula, see next section).

The theoretical phase diagram does not reproduce the congruent point where the two-phase region is reduced to one point and the order-disorder transition reaches a maximum temperature. Nevertheless, the general agreement between experiments and calculations is quite satisfactory, specially in view of the difficulty of the experiment (high absorption of Co) and in view of the many approximations inherent to our CVM model which neglects, (i) the concentration dependence of the pair interactions, (ii) the multiplet interactions, (iii) the effect of static displacements, and (iv) the contribution of vibrational entropies. A calculation taking into account a concentration variation of these interactions, or some multiplet interactions, should improve qualitatively this aspect. The important point is that, at the measurement stoichiometry, the agreement is very good.

B. Monte Carlo calculation

The pair interaction energies obtained experimentally have been used to calculate the order disorder transition tem-

perature at the stoichiometry $CoPt_3$ (noted AB_3) by a Monte-Carlo simulation of the disordering process of the ordered state. The model used has been described in details in previous papers.[52–54] The configuration energy is described through the Ising Hamiltonian of Eq. (9) with five energies (first, second, third, fourth, and sixth nearest neighbors). We have assumed the relation $V_{ij}^{AA}=V_{ij}^{BB}=-V_{ij}^{AB}=V_{ij}=1/4[V_{ij}^{AA}+V_{ij}^{BB}-2V_{ij}^{AB}]$ since it simplifies the algorithm and does not modify the transition temperatures.[52] In order to get the order-disorder critical temperature, we calculate the time dependence of the long-range order parameter $[\eta^T(t)]$ at various temperatures. The model is based on a vacancy-atom exchange mechanism between nearest neighbors, which has been proven to be dominant in metals at low temperatures.[55] The jump probability is given by a Glauber algorithm as a function of the energy change between the initial and final states ΔE. We have neglected the interaction energies between the vacancies and their neighboring atoms since, as shown previously,[53,54,21] such interactions have a negligible effect on T_C when the vacancy concentration is small (as it is the case in the $CoPt_3$ system[29,41]).

The crystal contains 32^3 $L1_2$ cells with periodic boundary conditions (the upper face atoms being considered as neighbors of the lower face atoms for example). The simulation starts with a perfect $L1_2$ ordered crystal in which one of the sublattices (sublattice α) is occupied by cobalt atoms and the other three by platinum atoms (inset of Fig. 4). Ten vacancies are introduced at random in the crystal. The vacancy concentration is kept constant during the simulation for all temperatures since we are only interested in the final equilibrium value of the long-range order parameter.

A Monte-Carlo step consists of the following: a vacancy and one nearest-neighbor site to this vacancy are chosen at random. If there is an atom on it, the energy change corresponding to the exchange between the vacancy and that particular atom is calculated and the jump is performed if the Glauber probability $P(\Delta E)=[1+\exp(\Delta E/k_BT)^{-1}]$ is larger than a random number between 0 and 1. This corresponds to averaging the result over a large number of reversal jump attempts, the sum of the probabilities of the jump and its reversal being equal to 1.

The long range order parameter is calculated at regular time intervals by counting the A atoms on the four different sublattices: $\eta=4/3(4N_A^{\alpha}-N_A)/(N_{\text{sites}}-N_{\text{vacancies}})$. For each temperature, the evolution of the order parameter is followed as long as it is necessary to reach equilibrium. The observed kinetics can be explained by the sum of two exponential laws (Fig. 7). The shorter relaxation time is almost constant and equal to 2×10^6 Monte-Carlo steps whereas the longer relaxation time varies between 5×10^6 and 2×10^8 Monte Carlo steps (the high value is indicative of a slowing down close to the order-disorder transition, see the inset of Fig. 7). We consider that equilibrium is reached when the simulation time is at least six times larger than the long relaxation time. We verify that the three other sublattices remain equivalent, to ensure that no large antiphase domain has appeared. Near the critical temperature, large fluctuations of the order parameter are indeed observed but, within the normal fluctuations due to the limited size of the sample, they remain equal for the three equivalent sublattices.

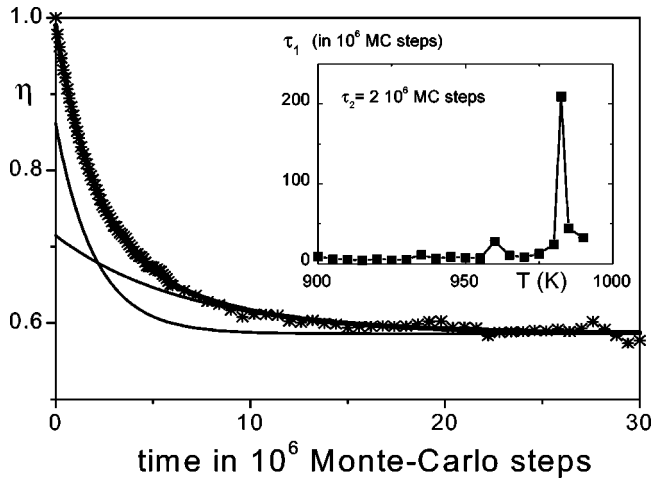

FIG. 7. Kinetics at 925 K and its simulation with two relaxation times. Inset: temperature dependence of the longer relaxation time.

The variation of the equilibrium order parameter as a function of temperature is shown on Fig. 8 by open squares. The transition seems to be very slightly of first order, taking place between 987.5 and 990 K, a temperature range much smaller than the one obtained in CVM. The method used to calculate the long range order parameter, which does not take into account the antiphase domains, only gives an estimate of the transition temperature.

The uncertainty in the critical temperature due to the experimental error in the pair interaction energy V_1 has been estimated by doing the simulation with all V_i's unchanged except for V_1 that was increased by ΔV_1 (filled circles in Fig. 8). We thus get an increment of the critical temperature of 23 K.

These results can be compared to the results of the Clapp and Moss formula,[56] which is the simplest statistical model that can be used to describe these order-disorder phenomena. In this model, the critical temperature is given by $k_BT_C=-4c(1-c)V(100)$ where k_B is the Boltzmann constant, c the concentration. $V(100)$ is the value of the Fourier transform of the pair interactions taken at the [100] reciprocal point, which is the superstructure peak of the $L1_2$ ordered

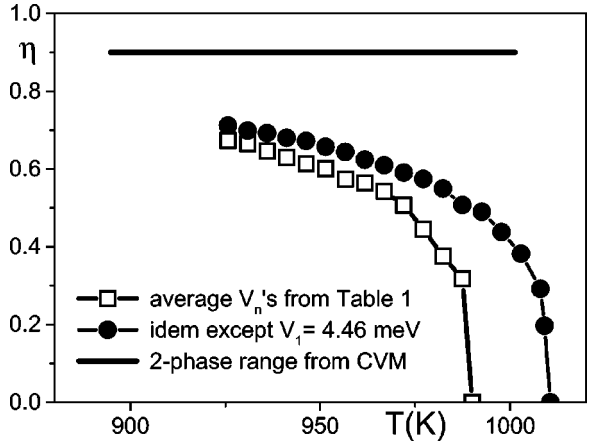

FIG. 8. Temperature variation of the long range order parameter η obtained by Monte Carlo simulations for the pair interactions in Table I and with V_1 replaced by $V_1+\Delta V_1$. The two phase range from CVM (bold line) is also represented.

phase. In this manner, we obtain the expression: $k_B T_C = -4c(1-c)(-4V_1+6V_2-8V_3+12V_4+8V_6)$ which leads to $T_C = 962$ K. This value is quite close to the value obtained by the Monte-Carlo simulations, which is expected to be a much better estimate.

The uncertainty in the critical temperature due to the errors in the pair interaction energies can be easily estimated using the Clapp and Moss formula. For V_1 we get 24 K, which is similar to the value found by the Monte Carlo simulation. We have estimated the other contributions to the error bar on T_C by this method and the results are given in Table I. The cumulative error is 118 K, assuming that the energy measurements are independent and that their squared errors can be added. Finally, we can give for the critical temperature $T_C = 990 \pm 120$ K, which compares well with the experimental value of $T_C = 978 \pm 8$ K (disordering process, see Fig. 6).

VI. CALCULATION OF ANTIPHASE BOUNDARY (APB) ENERGIES

The knowledge of the pair interaction energies gives access to the APB energies counting the associated change of the number of different pairs. We have focused on conservative antiphase boundaries (translation between the two domains parallel to the APB plane). In Ni_3V, that is ordered in the DO_{22} structure, Barrachin *et al.*[10] have shown that the energy of the conservative APB in the DO_{22} (100) plane is given by $\xi(100)_{DO_{22}} = 2V_2 - 8V_3 + 8V_4 + 8V_6$ limiting the development to the sixth nearest neighbors.

The same calculation gives the opposite of the (100) APB energy in the $L1_2$ phase, up to the sixth neighbors, as the $L1_2$ and DO_{22} structures are related by the introduction of (100) APB's and contain otherwise the same atomic environments: $\xi(100)_{L1_2} = -2V_2 + 8V_3 - 8V_4 - 8V_6$. With this formula, we get for $CoPt_3$: $\xi(100)_{L1_2} = 52 \pm 10$ meV per site of the APB. In the DO_{22} phase, Barrachin *et al.* obtained $\xi(100)_{DO_{22}} = 25$ meV in Ni_3V whereas Solal *et al.* obtained $\xi(100)_{DO_{22}} = 2.2$ meV in Pd_3V. The small value of the latter is in agreement with the degeneracy of $L1_2$ and DO_{22} structures in the Pd_3V compound. The high and positive value we obtain in $CoPt_3$ is consistent with the high stability of the $L1_2$ phase in this system, in agreement with the strong SRO intensity measured around the [100] point.

Similarly, we got the expression for a conservative APB along the most compact (111) planes in the $L1_2$ phase, counting the pair interaction energy changes $\xi(111)_{L1_2} = V_1 - 3V_2 + 4V_3 - 6V_4 + 6V_5 - 6V_6$. Assuming that V_5 is negligible we obtain for $CoPt_3$: $\xi(111)_{L1_2} = 52 \pm 8$ meV per APB site. This value is very close to $\xi(100)_{L1_2}$. This isotropy of the antiphase boundary energy explains why in $CoPt_3$ the APB's are not facetted [a wavy shape of APB's has been observed by TEM in $Co_{30}Pt_{70}$ (Ref. 32)].

VII. CONCLUSION

Diffuse scattering experiments provide a powerful experimental tool to study atomic interactions in alloys and, from them, phase stability as a function of temperature and composition.

In the present study, the neutron diffuse scattering results for the paramagnetic phase of a $CoPt_3$ alloy indicate relatively weak effective pair interactions (<10 meV) that extend to at least the fourth neighbor pairs. Nevertheless, strong statistical correlations are present even at high temperatures which, for all practical purposes, preclude the analysis of the SRO diffuse intensity by means of the conventional Krivoglaz-Clapp-Moss formula. Here we have used a 13-14 approximation of the CVM which allows us to extract up to sixth neighbor interactions minus the fifth one. The calculated Pt-rich side of the phase diagram, the order-disorder transition temperatures and the antiphase boundaries energies deduced from these interactions are in general agreement with experimental data. The important difference between the first pair interaction energy in Co_3Pt and $CoPt_3$ is attributed to a difference in *d*-band filling.

ACKNOWLEDGMENT

We gratefully acknowledge D. Stoeffler (IPCMS-GEMME) for providing us with a routine to obtain the intensity maps in Fig. 1.

*Present address: Institut für Festkörperforschung, Forschungszentrum Jülich, D-52425 Jülich, Germany.

[1] K. Masuda-Jido, R. Kikuchi, and R. Thomson, *Theory and Application of the Cluster Variation and Path Probability Methods* (Plenum, New York, 1996), p. 299.

[2] G.D. Garbulsky and G. Ceder, Phys. Rev. B **53**, 8993 (1996).

[3] J.D. Althoff, D. Morgan, D. de Fontaine, S. M. Asta, S. M. Foiles, and D. D. Johnson, Comput. Mater. Sci. **10**, 411 (1998), and references therein.

[4] R. Ravelo, J. Aguilar, M. Baskes, J.E. Angelo, B. Fultz, and B.L. Holian, Phys. Rev. B **57**, 862 (1998).

[5] A. van de Walle, G. Ceder, and U.V. Waghmare, Phys. Rev. Lett. **80**, 4911 (1998).

[6] V. Ozolins, C. Wolverton, and A. Zunger, Phys. Rev. B **58**, R5897 (1999).

[7] L. Shaojun, D. Suqing, and M. Benkun, Phys. Rev. B **58**, 9705 (1998).

[8] F. Solal, R. Caudron, F. Ducastelle, A. Finel, and A. Loiseau, Phys. Rev. Lett. **58**, 2245 (1987).

[9] F. Solal, R. Caudron, and A. Finel, in *Alloy Phase Stability*, edited by G.M. Stocks and A. Gonis, Vol. 163 of *NATO ASI Series E: Applied Sciences* (Kluwer, Dordrecht, 1989), p. 107.

[10] M. Barrachin, Ph.D. thesis, Paris VI, 1993; M. Barrachin, A. Finel, R. Caudron, A. Pasturel, and A. Francois, Phys. Rev. B **50**, 12 980 (1994).

[11] E. Cabet-Deliry, Ph.D. thesis, Paris VI, 1996; E. Cabet-Deliry, A. Pasturel, F. Ducastelle, and A. Loiseau, Phys. Rev. Lett. **76**, 3140 (1996).

[12] D. Le Bolloc'h, Ph.D. thesis, Paris VI, 1997; D. Le Bolloc'h, R. Caudron, and A. Finel, Phys. Rev. B **57**, 2801 (1998).

[13] B. Schönfeld, L. Reinhardt, and G. Kostorz, Phys. Status Solidi B **147**, 457 (1988).

[14] W. Schweika and H.G. Haubold, Phys. Rev. B **37**, 9240 (1988).

[15] L. Reinhard, B. Schönfeld, G. Kostorz, and W. Bürer, Phys. Rev. B **44**, 1727 (1990).

[16] L. Reinhard, J.L. Robertson, S.C. Moss, G.E. Ice, P. Zschack, and C.J. Sparks, Phys. Rev. B **45**, 2262 (1992).
[17] V. Pierron-Bohnes, E. Kentzinger, M.C. Cadeville, J. Sanchez, R. Caudron, F. Solal, and R. Kozubski, Phys. Rev. B **51**, 5760 (1995).
[18] W. Schweika, in *Neutron Scattering for Material Science*, edited by S. M. Shapiro, S. C. Moss, and J. D. Jorgensen, MRS Symposia Proceedings No. 166, (Materials Research Society, Pittsburgh, 1990), p. 249.
[19] V. Pierron-Bohnes, S. Lefebvre, M. Bessière, and A. Finel, Acta Metall. Mater. **34**, 2701 (1990).
[20] V. Pierron-Bohnes, M.C. Cadeville, A. Finel, and O. Schaerpf, J. Phys. (France) **1**, 1247 (1991).
[21] E. Kentzinger, Ph.D. thesis, University Louis Pasteur, Strasbourg, 1996.
[22] M. Bessière, Y. Calvayrac, S. Lefebvre, D. Gratias, and P. Cénédèse, J. Phys. (France) **47**, 1961 (1986).
[23] B.D. Butler and J.B. Cohen, J. Appl. Phys. **65**, 2214 (1986).
[24] F. Chassagne, M. Bessière, Y. Calvayrac, P. Cénédèse, and S. Lefebvre, Acta Metall. **14**, 367 (1989).
[25] L. Anthony, L.J. Nagel, J.K. Okamoto, and B. Fultz, Phys. Rev. Lett. **22**, 3034 (1994).
[26] L.J. Nagel, L. Anthony, and B. Fultz, Philos. Mag. Lett. **72**, 421 (1995).
[27] P.D. Bogdanoff, B. Fultz, and S. Rosenkranz, Phys. Rev. B **60**, 3976 (1999).
[28] L. Anthony, J.K. Okamoto, and B. Fultz, Phys. Rev. Lett. **70**, 1128 (1993).
[29] C.E Dahmani, Ph.D. thesis, University Louis Pasteur Strasbourg, 1985.
[30] M.C. Cadeville, C.E. Dahmani, and F. Kern, J. Magn. Magn. Mater. **54-57**, 1055 (1986).
[31] C. Leroux, Ph.D. thesis, University Louis Pasteur Strasbourg, 1989.
[32] C. Leroux, A. Loiseau, M.C. Cadeville, D. Broddin, and G. Van Tendeloo, J. Phys.: Condens. Matter **2**, 3479 (1990).
[33] L. Bouzidi, M.C. Cadeville, and V. Pierron-Bohnes, in *Solid-Solid Phase Transformations*, edited by W.C. Johnson, J.M. Howe, D.E. Laughlin, and W.A. Soffa (The Minerals, Metals and Materials Society, Warrendale, PA, 1994), pp. 431–436.
[34] G. Inden, in *Alloy Phase Diagram*, edited by L.H. Bennett, T.B. Massalski, and B.C. Giessen, MRS Symposia Proceedings No. 19 (Materials Research Society, Pittsburgh, 1983), p. 175.
[35] J.M. Sanchez, J.L. Moran-Lopez, C. Leroux, and M.C. Cadeville, J. Phys. C **8**, 107 (1988).
[36] A. Bieber and F. Gautier, J. Phys. Soc. Jpn. **53**, 2061 (1984); Z. Phys. B: Condens. Matter **57**, 335 (1984).
[37] M. Capitan, S. Lefebvre, Y. Calvayrac, M. Bessière, and P. Cénédèse, J. Appl. Crystallogr. **32**, 1039 (1999).
[38] V. Parasote, Ph.D. thesis, University Louis Pasteur Strasbourg, 1998; V. Parasote *et al.* (unpublished).
[39] E. Kentzinger and H.R. Schober (unpublished).
[40] H. Berg and J.B. Cohen, Metal Trans. **3**, 1797 (1972).
[41] C.E. Dahmani, M.C. Cadeville, and V. Pierron-Bohnes, Acta Metall. Mater. **33**, 369 (1985).
[42] P. Barberis, Ph.D. thesis, Orsay, 1992.
[43] I.A. Blech and B.L. Averbach, Phys. Rev. B **137**, 1113 (1965).
[44] K.A. Gschneidner, Solid State Phys. **16**, 276 (1964).
[45] M.A. Krivoglaz, *Theory of X-Ray and Thermal Neutrons Scattering by Real Crystals* (Plenum Press, New York, 1969).
[46] V.F. Sears, Neutron News **3**, 26 (1992).
[47] B. Borie and C.J. Sparks, Acta Crystallogr., Sect. A: Cryst. Phys., Diffr., Theor. Gen. Crystallogr. **27**, 198 (1971).
[48] J.M. Cowley, J. Appl. Phys. **21**, 24 (1950).
[49] V. Pierron-Bohnes, C. Leroux, J.P. Ambroise, A. Menelle, and P. Bastie, Phys. Status Solidi A **116**, 529 (1989).
[50] D. Gratias and P. Cénédèse J. Phys. (France) **46**, C9-149 (1985).
[51] A. Finel, in *Statics and Dynamics of Alloy Phase Transformations*, edited by P.E.A. Turchi and A. Gonis, Vol. 319 of *NATO Advanced Study Institute, Series B: Physics* (Plenum, New York, 1994), p. 495.
[52] K. Yaldram, V. Pierron-Bohnes, M.C. Cadeville, and M.A. Khan, J. Mater. Res. **10**, 591 (1995).
[53] E. Kentzinger, V. Pierron-Bohnes, M.C. Cadeville, M. Zemirli, H. Bouzar, M. Benakki, and M.A. Khan, Defect Diffus. Forum **143-147**, 333 (1997).
[54] E. Kentzinger, M. Zemirli, V. Pierron-Bohnes, M.C. Cadeville, H. Bouzar, M. Benakki, and M.A. Khan, Mater. Sci. Eng., A **239-240**, 784 (1997).
[55] W. Petry, A. Heiming, C. Herzig, and J. Trampenau, Defect Diffus. Forum **75**, 211 (1991).
[56] P.C. Clapp and S.C. Moss, Phys. Rev. **171**, 754 (1968).